Hierarchically Porous Reduced Graphene Oxide Coated with Metal–Organic Framework HKUST-1 for Enhanced Hydrogen Gas Affinity

Kyung Seob Song,[†] Daeok Kim,[‡] and Ali Coskun*[,†]

[†]Department of Chemistry, University of Fribourg, Fribourg 1700, Switzerland

[‡]Graduate School of EEWS, Korea Advanced Institute of Science and Technology, 373-1 Guesong Dong, Daejeon 305-701, Republic of Korea

Supporting Information

ABSTRACT: Metal–organic frameworks (MOFs) are crystalline porous materials that have been actively explored for various gas storage, separation, and conversion applications because of their structural tunability. While the micropores (<2 nm) in MOFs are essential for increased gas affinity, these small pores significantly decrease the mass-transport kinetics. One way to address this challenge is to develop hierarchically porous MOFs with interconnected micro-, meso-, and macropores. Whereas these MOFs can be formed by using soft/hard templates or by creating pores through postmodification, they can also be achieved by growing them on structural templates such as porous carbons, i.e., reduced graphene oxide. The latter strategy can enable the introduction of hierarchical porosity while creating a synergistic effect to simultaneously improve both the mechanical property and gas affinity by creating pores at the interface. In this direction, we demonstrated that the coating of HKUST-1 onto a hierarchically porous reduced graphene oxide (HRGO) led to the formation of a hierarchically porous structure, namely, HKUST-1@HRGO, with increased affinity toward H_2 gas. While the isosteric heats of adsorption (Q_{st}) values for H_2 were found to be 7.7, 6.9, and 6.7 kJ mol^{-1} for HRGO, HKUST-1, and the physical mixture of HKUST-1 and HRGO, respectively, at zero coverage, that of the HKUST-1@HRGO composite revealed a significant increase of up to 9.26 kJ mol^{-1}, thus clearly demonstrating not only the synergetic effect between HKUST-1 and the reduced graphene oxide but also the critical role of interfacial pores as high-affinity binding sites.

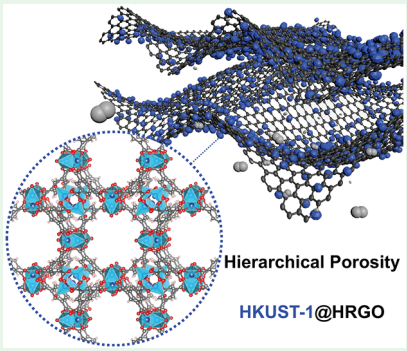

KEYWORDS: *metal–organic frameworks, gas storage, hierarchical porosity, H_2 storage, graphene*

INTRODUCTION

Metal–organic frameworks (MOFs) are highly crystalline porous materials involving the linkage of preorganized metal clusters and organic linkers. Considering the myriad of possibilities in terms of organic linkers as well as metal clusters, the chemical nature, size, and shape of the pores can be tuned for the desired application such as hydrogen (H_2) storage,[1−3] carbon dioxide (CO_2) capture and conversion,[4] methane storage,[5] gas separation,[6,7] water harvesting,[8] enzyme encapsulation,[9] and heterogeneous catalysis.[10,11] Along these lines, efficient H_2 storage at either room temperature or cooler temperatures is still an important challenge, yet to tackled, for porous materials in general. Growing environmental concerns originating from increased CO_2 emissions into the atmosphere rendered H_2 fuel cell cars as viable alternatives for transportation. The state-of-the-art storage systems require ultrahigh pressures of up to 700 bar and entail special, rather expensive carbon-reinforced composite tanks in a cylindrical shape. The goal for H_2 storage using porous materials is to realize the same amount of H_2 storage capacity as those of high-pressure systems at much lower pressures, e.g., 100 bar, thus eliminating the material, shape, and size restrictions of the storage tanks and decreasing the overall cost significantly. The good reversibility for H_2 storage at room temperature requires a H_2 binding enthalpy in the range of 15−20 kJ mol^{-1}. Considering the low polarizability of H_2, the structures should involve either open metal sites[12,13] or ultrafine pores near the kinetic diameter (2.76 Å) of H_2 gas or ideally a combination of both.

In this direction, HKUST-1 containing a copper paddle-wheel cluster and a 1,3,5-benzenetricarboxylate linker has been actively investigated[1] in H_2 storage because of its open metal sites, Cu^{2+}, and micropores (10 and 14 Å) along with a high surface area.[14] Notably, comparative analysis of a copper paddle-wheel-based MOF, namely, SNU-5, with/without open metal sites, showed a 10−20% H_2 uptake difference per volume in the same structure and a 5.07 kJ mol^{-1} difference in the binding enthalpy (at zero coverage), reaching up to 11 kJ mol^{-1} for the one with open metal sites.[15] HKUST-1 showed a relatively modest H_2 binding enthalpy of 6.9 kJ mol^{-1}.[16] In order to further increase the H_2 affinity of HKUST-1, we recently showed that the incorporation of palladium/copper

Scheme 1. (a) Schematic Representation of a HKUST-1 Coating on HRGO and (b) Two-Step Coating Mechanism of HKUST-1 on the HRGO Surface

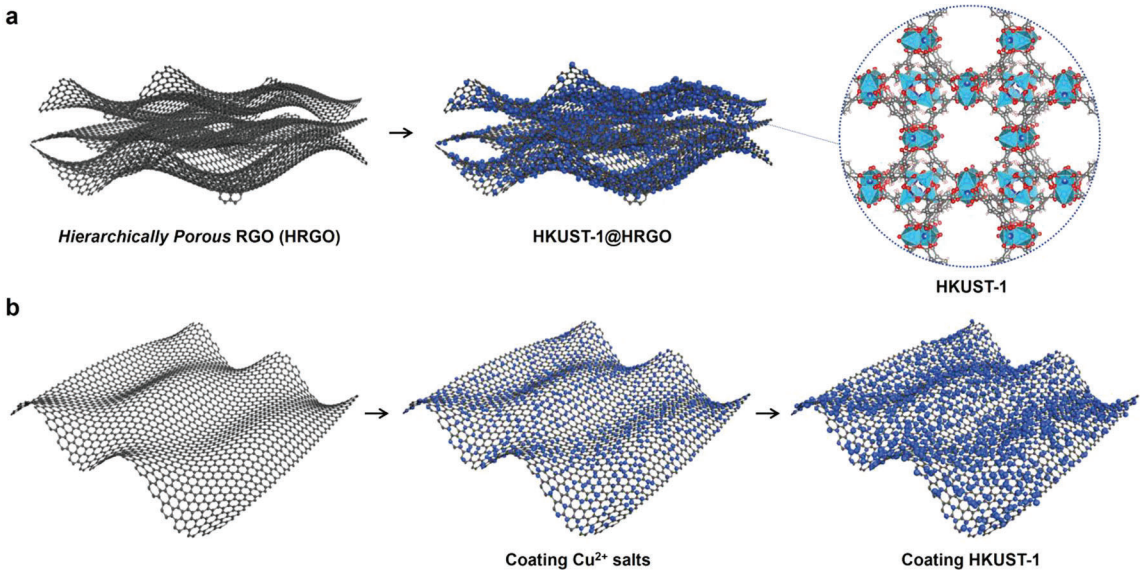

paddle-wheel structures into HKUST-1 increases the H_2 binding enthalpy by up to 3 kJ mol^{-1}. This particular MOF, however, has been shown to degrade upon exposure to H_2 at room temperature.[17]

Generally, microporous materials do not allow fast gas diffusion, which significantly slows gas uptake/release kinetics. In this sense, the formation of a hierarchically porous structure can be a good direction.[18] Hierarchically porous structures contain interconnected micro-, meso-, and macropores; while micropores provide high affinity toward guest molecules, mesopores facilitate fast diffusion and mass transport. Accordingly, various synthetic strategies for the synthesis of hierarchically porous MOFs have been developed.[19−21] These strategies include linker labilization,[22] steric index control of the linker,[23] defect engineering,[24] selective acid etching,[25] polystyrene[26] and supramolecular templation.[27−29]

MOF/graphene composites, i.e., graphene oxide, graphite oxide, and reduced graphene oxide, have been investigated as structural templates to improve the mechanical strength, stability, conductivity, and gas affinity of MOFs.[30−38] These composite structures have been shown to inherit[35] the mechanical stability of graphene, while the extended π surface area increased the gas affinity, electrical conductivity,[31,36] and molecule adsorption ability.[34,38] Notably, these porous graphenes also served as structure-directing agents for efficient morphology control.[31,37] In an effort to understand the impact of interfacial pore formation between MOFs and a graphene template on the gas affinity, herein, we report (Scheme 1) the preparation of a hierarchically porous MOF/graphene composite by growing HKUST-1 on a structural template, that is, hierarchically porous reduced graphene oxide (HRGO). The resulting HKUST-1@HRGO showed significantly improved binding enthalpy of H_2, up to 9.26 kJ mol^{-1}, compared to both HKUST-1 and HRGO, thus highlighting the synergetic effect between HKUST-1 and HRGO as well as the importance of interfacial pores in tuning the gas affinity, which is further verified by increasing the binding enthalpy of H_2 at zero coverage with increasing HRGO content.

RESULTS AND DISCUSSION

First, we investigated the growth of HKUST-1 on HRGO in a one-pot reaction. However, this approach primarily led to the formation of individual micron-sized HKUST-1 crystals rather than a coating on the HRGO surface. Therefore, in order to achieve homogeneous growth of HKUST-1 on the reduced graphene oxide surface, a two-step synthetic approach was adopted (Scheme 1b).[39] We also varied the HRGO amount (10, 15, and 20 wt %) with a fixed amount of HKUST-1 reactants to investigate the impact of the structural template on the textural properties and gas affinity.

We coated the HRGO surface with excess $Cu(OAc)_2{\cdot}xH_2O$ in a solvent mixture of dimethylformamide (DMF), ethanol (EtOH), and deionized (DI) water, followed by the addition of 1,3,5-benzenetricarboxylic acid (BTC) in the same solvent mixture and triethylamine (Et_3N). The resulting mixture was stirred under ambient conditions for 24 h. Then, the reaction mixture was centrifuged with EtOH until the solution color became transparent. This washing step was performed in order to remove unreacted salts and organic linkers.

In order to verify the growth of HKUST-1 on HRGO, we conducted powder X-ray diffraction (PXRD) analysis (Figure 1). The characteristic diffraction peaks of HKUST-1[14,31] were observed in all of the HKUST-1@HRGO samples, pointing to the successful formation of crystalline HKUST-1 on HRGO. Overall, increasing the HRGO amount in the HKUST-1@HRGO composite led to a decrease in the intensities of the diffraction peaks while increasing the peak broadness. We attribute this result to the fact that the solid interphase of the template can influence the nucleation rate and MOF growth mechanism (heterogeneous nucleation).[40] We speculate that the curved surface of HRGO might cause a disorder in the HKUST-1 structure.[32]

To evaluate the chemical connectivity and morphology of HKUST-1@HRGO, Fourier transform infrared spectroscopy (FT-IR), X-ray photoelectron spectroscopy (XPS), scanning electron microscopy (SEM), and energy-dispersive X-ray (EDX) spectroscopy analyses were performed. FT-IR analysis of HRGO revealed a C═C stretching band at 1561 cm^{-1}

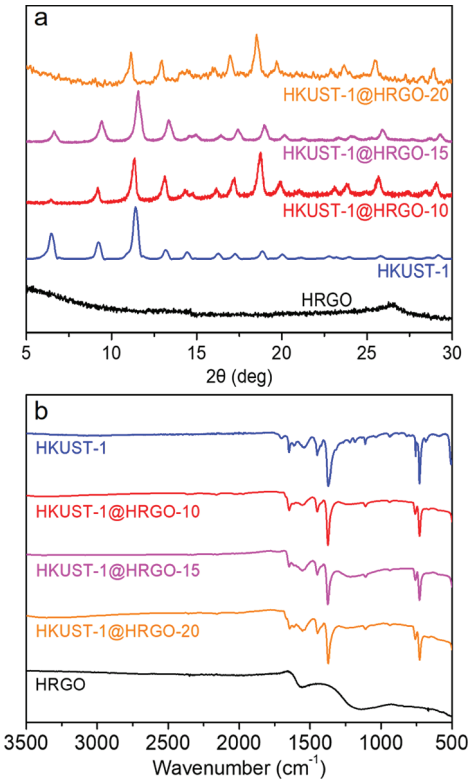

Figure 1. (a) PXRD and (b) FT-IR analyses of HRGO, HKUST-1, and HKUST-1@HRGO with varying HRGO loadings.

along with a C−O−C stretching band at around 1200 cm^{-1} as broad peaks[41] (Figure 1). We were unable to observe the carboxylic acid band in the FT-IR spectrum, but its existence can be verified by XPS C 1s analysis (288.4 eV; Figure S1). Following the growth of HKUST-1 on HRGO (Figure 1b), asymmetric stretching (1652 and 1559 cm^{-1}), symmetric vibration (1449 and 1368 cm^{-1}), and out-of-plane vibrational bands of carboxylate groups (718 cm^{-1}) were observed in the FT-IR spectrum. Importantly, we observed a slightly decreased C−O−C stretching band at around 1200 cm^{-1} in HKUST-1@HRGOs and a Cu−O stretching band at 479 cm^{-1}, which can be interpreted as both the coordination of a HRGO surface oxygen atom to copper(2+) as well as the formation of metal clusters.[30,31,34] We compared the XPS spectra (C 1s, O 1s, and Cu 2p) of HKUST-1@HRGO with those of the physical mixture of HKUST-1 and HRGO (Figure S2 and Table S1), and we observed a slight shift, from 533.6 to 531.7 eV, in the O 1s binding energy for the surface oxygen atoms in HKUST-1@HRGO, thus supporting the presence of a strong interaction between HKUST-1 and HRGO. The oxygen content of HRGO was analyzed by thermal gravimetric analysis (TGA) and found to be 15.7 wt % (Figure S3). In order to quantify the exact amount of copper(2+) in HKUST-1@HRGOs, we conducted inductively coupled plasma optical emission spectrometry (ICP-OES) analysis (Table S2 and Figure S4). We observed a decrease in the copper(2+) content (11.5, 8.5, and 5.7 wt % for HKUST-1@HRGO-10, HKUST-1@HRGO-15, and HKUST-1@HRGO-20, respectively) with increasing HRGO loading. In addition, a physical mixture of HKUST-1 and HRGO showed lower copper and oxygen contents compared to those of HKUST-1@HRGOs (Table S1), which indicates that a two-step synthetic approach facilitates the chemical connectivity between HKUST-1 and HRGO.

Surface Coating Mechanism of HKUST-1@HRGO. In order to understand the surface coating mechanism, we performed SEM analysis (Figures 2 and 3). SEM analysis of HRGO revealed wrinkled reduced graphene oxide with cabbage-like morphology (Figure 2a). Importantly, HRGO showed micron-sized intrinsic voids. Following HKUST-1 growth on the HRGO surface, the cabbage-like morphology of HRGO is retained (Figure 2b,c). EDX spectroscopy mapping of copper(2+) in both HRGO and HKUST-1@HRGO

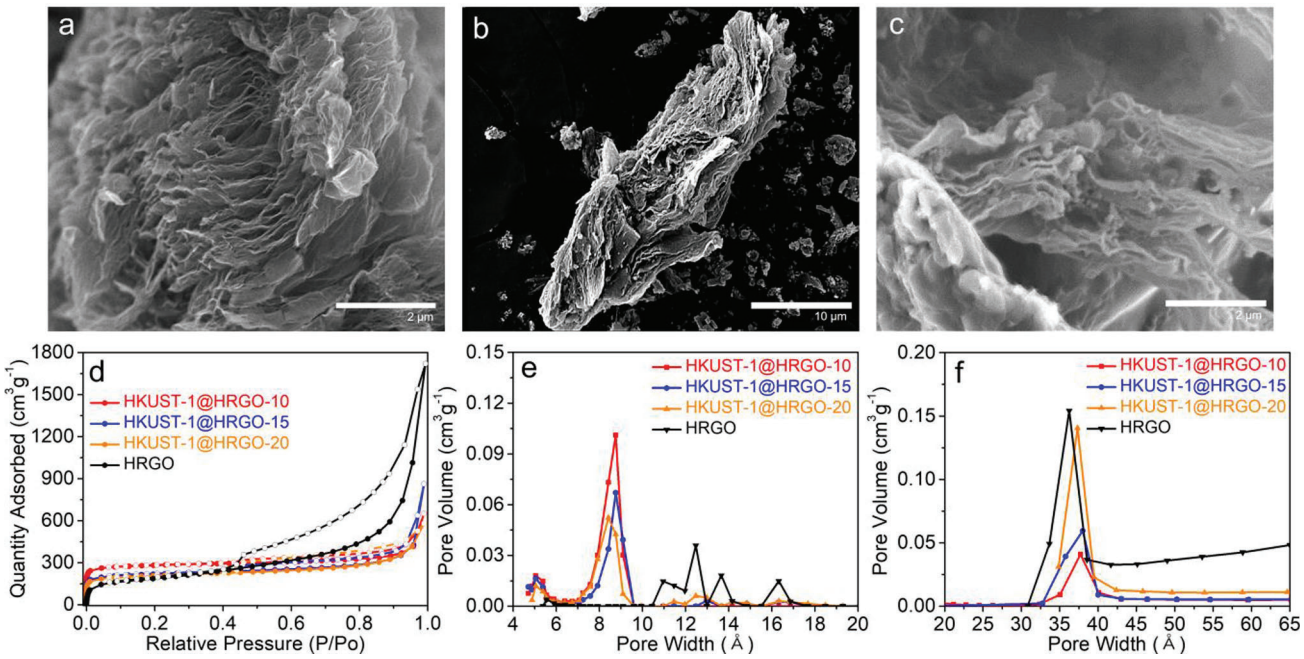

Figure 2. SEM images of (a) HRGO and (b and c) HKUST-1@HRGO. (d) Argon adsorption (filled)−desorption (empty) isotherms of HRGO, HKUST-1@HRGO-10, -15, and -20 at 87 K along with (e and f) PSDs calculated by NLDFT.

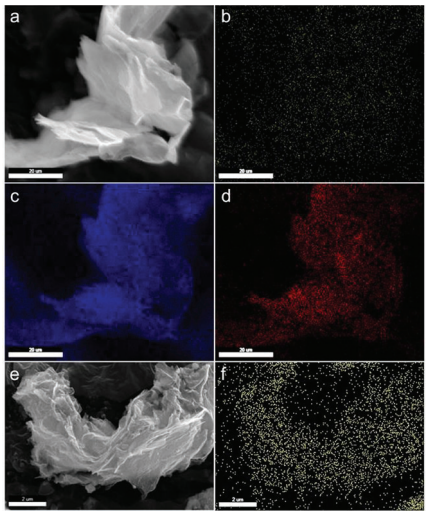

Figure 3. SEM image of (a) Cu@HRGO (top view). EDX images of (b) copper, (c) carbon, and (d) oxygen. (e) SEM image of HKUST-1@HRGO (top view). (f) EDX image of copper.

showed good chemical compatibility of copper(2+) and verified its homogeneous distribution (Figure 3). To investigate the HKUST-1 coating mechanism, we performed SEM analysis after 1, 2, 4, and 8 h of reaction without a washing step (Figure S5). With increasing reaction time, we observed a higher copper intensity in the EDX analysis. Even after 1 h, the surface of HRGO was already coated with nanosized HKUST-1 seeds. We can also observe growth of HKUST-1 on the HRGO surface (after 2 h). After saturation of the HRGO surface with HKUST-1 crystals, the HKUST-1 nanoparticles started to grow and fill the macro/mesopores in HRGO (after 4 h). The size of the HKUST-1 particles significantly increased after 8 h. The excess HKUST-1 particles were removed by centrifugation and a washing process. The fast nucleation of the HKUST-1 nanoparticles was suggested to originate from a heterogeneous nucleation and growth process. The defects (e.g., edges of nanopores and oxygen functional groups) and wrinkled/curved surface of HRGO offer multiple nucleation spots for the HKUST-1 nanoparticles, thus leading to the formation of interfacial pores (Figures S6 and S7).

Textural Properties of HKUST-1@HRGO. To verify the formation of a hierarchically porous structure, HKUST-1@HRGOs were characterized by Brunauer–Emmett–Teller (BET) analysis at 87 K using argon (Figures 2 and S8). An argon adsorption–desorption isotherm of HRGO exhibited a type IV isotherm with a broad H3-type hysteresis in a desorption branch at above $P/P_o = 0.4$, which is a characteristic feature of the presence of mesopores. H3-loop-type hysteresis is usually observed from slit-shaped pores and nonrigid frameworks. In addition, the fast gas uptake at the low-pressure range indicated the presence of micropores, thus verifying the formation of a hierarchically porous structure with a BET surface area of 586 $m^2\ g^{-1}$ (Figure 2 and Table 1). The origin of the porosity in HRGO is the evolution of gaseous species (CO_2 and CO) during thermal annealing of graphene oxide.[36] Additionally, this phenomenon led to the formation of open, stacked 2D reduced graphene oxide layers, thus creating hierarchical pores in HRGO (Figure 2a). Moreover, HRGO showed a very high pore volume of 2.1 $cm^3\ g^{-1}$ accompanied by a low micropore volume of 0.045 $cm^3\ g^{-1}$ calculated from the *t*-plot analysis. HRGO showed (Figure 2f) an average mesopore size of 36 Å along with micropores in the range of 10–16 Å calculated by nonlocal density functional theory (NLDFT).

Table 1. BET Analysis of the HRGO and HKUST-1@HRGO series

sample	BET[a] ($m^2\ g^{-1}$)	S_{micro}[b] ($m^2\ g^{-1}$)	S_{ext}[c] ($m^2\ g^{-1}$)	V_{total}[d] ($cm^3\ g^{-1}$)	V_{micro}[e] ($cm^3\ g^{-1}$)	V_{ext}[f] ($cm^3\ g^{-1}$)
HRGO	586	136	450	2.1	0.045	1.97
HKUST-1@HRGO-10	918	751	167	0.81	0.34	0.47
HKUST-1@HRGO-15	706	515	191	1.08	0.25	0.83
HKUST-1@HRGO-20	670	470	200	0.73	0.24	0.49

[a]BET surface area calculated over the pressure range (P/P_0) of 0.01–0.11. [b]Micropore surface area calculated using the *t*-plot method. [c]$S_{ext} = S_{total} - S_{micro}$. [d]Total pore volume obtained at $P/P_0 = 0.99$. [e]Micropore volume calculated using the *t*-plot method. [f]$V_{ext} = V_{total} - V_{micro}$.

The growth of HKUST-1 on the surface of HRGO resulted in significant changes in its textural property (Figure 2d). Compared to HRGO, HKUST-1@HRGO-10 exhibited a type I isotherm with a H4-type hysteresis loop, which is generally observed for micro/mesoporous adsorbents. While HKUST-1 growth significantly increased the micropore content (<0.3 P/P_0), it simultaneously decreased the mesopore content of HRGO (Figure S9), e.g., 136 $m^2\ g^{-1}$ (S_{micro}) and 0.045 $cm^3\ g^{-1}$ (V_{micro}) for HRGO and 751 $m^2\ g^{-1}$ (S_{micro}) and 0.34 $cm^3\ g^{-1}$ (V_{micro}) for HKUST-1@HRGO-10, thus verifying the filling of mesopores in HRGO with HKUST-1. Notably, the pore size of 9 Å was consistently observed for all of the HKUST-1@HRGO series (Figure 2e), which is well-matched with the small pores of HKUST-1.[14] These results collectively suggest the formation of hierarchically porous HKUST-1@HRGO composites with interconnected micro-, meso-, and macropores.

To study the effect of HKUST-1 coating on HRGO, we systematically varied the HRGO loading (10, 15, and 20 wt %) in HKUST-1@HRGO. After HKUST-1 coating, we observed higher surface areas for all HKUST-1@HRGOs compared to the surface area of HRGO. Among the HKUST-1@HRGOs, however, increasing the HRGO amount was found to decrease (Table 1) the surface area presumably because of the increased number of defect sites. We also observed distinct changes in the pore-size distribution (PSD). Whereas the percentage of 9-Å-sized pores decreased, the 36-Å-sized pores were found to increase (Figure 2e,f). We attributed this result to the presence of more heterogeneous nucleation spots at high HRGO loadings and the higher number of structural defects. S_{micro}/S_{ext} ratios were also found to decrease with increasing HRGO loadings (4.5, 2.7, and 2.35 for HKUST-1@HRGO-10, -15, and -20, respectively). In order to evaluate the water stability of HKUST-1@HRGO, we immersed both HKUST-1 and HKUST-1@HRGO in water and measured their BET surface areas afterward. Both samples showed substantially decreased surface areas. We believe that, because the HKUST-1 particles primarily located on the surface of HRGO, the hydrophobicity of the HRGO layer did not improve the water stability of the HKUST-1 coating (Figure S10).

H_2 Uptake of Hierarchically Porous HKUST-1@HRGOs. Recently, hierarchically porous graphenes with high pore

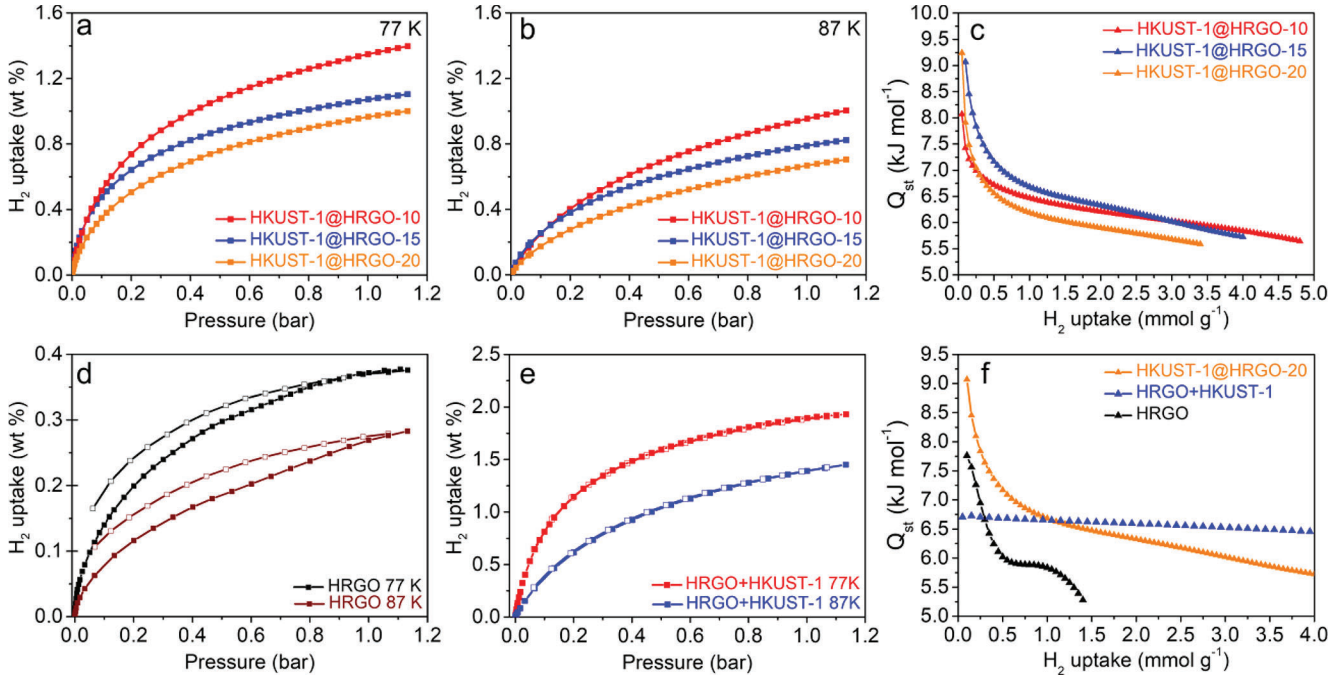

Figure 4. H_2 uptake at (a) 77 and (b) 87 K. (c) Q_{st} values of H_2 in the HKUST-1@HRGO series. (d) H_2 uptake of HRGO, (e) H_2 uptake of the physically mixed HRGO and HKUST-1. (f) Comparison of Q_{st} values of H_2 for HRGO, HRGO+HKUST-1, and HKUST-1@HRGO-20.

volumes were shown to exhibit improved gas uptake capacities.[42] Importantly, the synergistic effect of HKUST-1 and HRGO at the interface is expected to significantly improve H_2 affinity via the generation of interfacial pores featuring both a highly polarized extended π surface area and open metal sites.

H_2 uptake analysis is performed at 77 and 87 K. HRGO showed 0.38 and 0.28 wt % of H_2 uptake at 1.1 bar (Figure 4), at 77 and 87 K, respectively. The desorption isotherms of HRGO do not close, which is a characteristic feature of a flexible porous structure. Following HKUST-1 growth in HRGO, the H_2 uptake capacity significantly increased to 1.38 wt % for HKUST-1@HRGO-10, 1.1 wt % for HKUST-1@HRGO-15, and 1.0 wt % for HKUST-1@HRGO-20 at 77 K and 1.1 bar (Figure 4a). The growth of microporous HKUST-1 contributed to the improved H_2 uptake capacity of a hierarchically porous MOF/graphene composite. Compared to HKUST-1 (from 2.18 to 3.6 wt % of H_2 uptake at 77 K from 1 to 50 bar[43,44]), HKUST-1@HRGOs showed lower H_2 uptake capacities because of the fact that the heterogeneous nucleation of HKUST-1 on the HRGO surface led to both lower crystallinity and BET surface area compared to those of the pristine HKUST-1. Isosteric heats of adsorption (Q_{st}) values show the affinity of gas molecules toward the sorbent. Especially, the affinity of H_2 toward HKUST-1@HRGO was significantly improved compared to that of HRGO, 9.26 kJ mol^{-1} at zero coverage of HKUST-1@HRGO-20 and 7.7 kJ mol^{-1} at zero coverage of HRGO (Figure 4f). Whereas the profile of Q_{st} of H_2 in HKUST-1@HRGO represents both HKUST-1 and HRGO at high loadings, the difference originating from interfacial pores becomes evident at zero coverage, which is further supported by increasing Q_{st} of H_2 with increasing HRGO loadings in HKUST-1@HRGO. Furthermore, we also investigated the physical mixture of HKUST-1 and HRGO (Figure 4e). This mixture exhibited (Figure 4f) a Q_{st} value of only 6.7 kJ mol^{-1}, which is similar to that of HKUST-1 (6−7 kJ mol^{-1}).[16,43] These results show that HKUST-1 growth, its chemical bonding with the HRGO surface, and the formation of pores at the interface are key steps in controlling the H_2 affinity. Notably, after H_2 uptake analysis, we observed a slight increase in the BET surface area, pointing to both the stability and flexibility of the MOF/graphene composite (Table S3).

CONCLUSION

In this study, we demonstrated a facile strategy for the preparation of hierarchically porous MOFs by using porous reduced graphene oxide as a structural template. This approach allowed us to tune the porosity, morphology, and gas uptake behavior of the MOF. In addition, the critical role of the interfacial pores formed upon the growth of HKUST-1 on the surface of HRGO featuring both a highly polarized extended π surface area and open metal sites in tuning the H_2 affinity was clearly demonstrated. Because of its modularity, the present strategy can be extended to various MOFs to tune their gas affinity and uptake characteristics.

EXPERIMENTAL SECTION

Materials. All purchased chemicals are used without further purification. Graphite powder (Asbury Carbon), sulfuric acid (98%, Simga Aldrich), potassium permanganate (99.0%), BTC (99%, Sigma-Aldrich), $Cu(OAc)_2{\cdot}xH_2O$ (Sigma-Aldrich, 98%), Et_3N (99%, Sigma-Aldrich), DMF (Sigma-Aldrich), EtOH (Sigma-Aldrich), and deionized (DI) water.

Characterization. SEM and EDX spectroscopy mapping analyses were conducted using Magellan 400 (FEI). FT-IR spectra were measured using Bruker Alpha with 64 scan times and 2 cm^{-1} resolution. PXRD analysis was conducted using *SmartLab* (Rigaku) with Cu Kα radiation (λ = 1.5406 Å) at a generator voltage of 40 kV and a generator current of 200 mA. Argon isotherms at 87 K and H_2 isotherms at 77 and 87 K were measured using a 3Flex physisorption analyzer (Micromeritics, USA). To analyze the pore properties from the obtained isotherms, NLDFT adopting a carbon slit pore model was employed. XPS analysis was conducted using multipurpose XPS

(Sigma Probe, Thermo VG Scientific; X-ray source, monochromatic Al Kα).

Synthesis of Graphene Oxide. Graphene oxide was synthesized via a modified Hummers method.[45] Graphite powder (1 g, Asbury Carbon) was added to sulfuric acid (98%, 150 mL). Potassium permanganate (99.0%, 3.5 g) was gradually poured into the graphite/sulfuric acid solution, with vigorous stirring for 10 min at room temperature. After stirring for 2 h in an oil bath at 35 °C, the solution was placed in an ice bath and slowly diluted with 200 mL of DI water. A total of 50 mL of hydrogen peroxide was slowly added to the reaction mixture. The resulting product was filtered with filter paper and washed several times with diluted hydrochloric acid (10 v/v %), followed by freeze-drying to yield 1.5 g of a graphene oxide powder.

Thermal Annealing of Graphene Oxide for HRGO. We followed a previously reported procedure.[36] Graphene oxide powder was loaded into a quartz tube under a N_2 atmosphere. The quartz tube was then placed in a furnace, which was heated up to 650 °C (3 °C min^{-1}). The sample was kept at this temperature for 10 min, the tube was pulled from the furnace and rapidly cooled to room temperature.

MOF Growth on HRGO. BTC (50 mg, 0.238 mmol) was dissolved in 1.2 mL of a mixture of solvents, 0.4 mL each of DMF, EtOH, and DI water. The resulting mixture was sonicated for 1 min in order to obtain a homogeneous solution. A solution of $Cu(OAC)_2 \cdot xH_2O$ (50 mg, 0.25 mmol) in 1.2 mL of a mixture of solvents (0.4 mL each of DMF, EtOH, and DI water) was prepared, mixed with varying amounts of HRGO (20, 15, and 10 mg to achieve 20, 15, and 10 wt % with respect to the weight of the HKUST-1 reactants, respectively), and stirred for 10 min. The two solutions were then combined and stirred for an additional 10 min. At this point, Et_3N (0.05 mL) was added to the reaction mixture and stirred at room temperature for 24 h. In order to remove unreacted monomers, the reaction mixture was centrifuged with EtOH until the solution color became transparent. The resulting MOF composite was then dried at 40 °C for 12 h.

Preparation of Physically Mixed HKUST-1/HRGO. HKUST-1 (50 mg), which synthesized under the same experimental conditions as those of HKUST-1@HRGO, was dispersed in 1.2 mL of a solvent mixture of DMF/EtOH/H_2O (1:1:1) and added to HRGO (10 mg) in the same solvent mixture (1.2 mL). The resulting mixture was stirred for 24 h at room temperature. The products were centrifuged, washed several times with EtOH, and dried under a vacuum.

Analysis of H_2 Uptake. The dual-site Langmuir–Freundlich expression was used to fit all H_2 isotherm data at 77 and 87 K, where n is the amount adsorbed (mmol g^{-1}), n_{sat} is the saturation loading (mmol g^{-1}), b_i is the Langmuir parameter (bar^{-vi}), p is the pressure, and v_i is a constant for sites 1 and 2

$$n = \frac{n_{sat,1} b_1 p^{v_1}}{1 + b_1 p^{v_1}} + \frac{n_{sat,2} b_2 p^{v_2}}{1 + b_2 p^{v_2}}$$

Q_{st} was calculated for each material with the fitting plots and using the Clausius–Clapeyron relationship, where R is the ideal gas constant, p is the pressure, and T is the temperature.

$$-Q_{st} = RT^2 \left(\frac{\partial \ln p}{\partial T} \right)_n$$

■ ASSOCIATED CONTENT

Supporting Information

The Supporting Information is available free of charge at https://pubs.acs.org/doi/10.1021/acsanm.9b01973.

XPS analysis, survey spectra, TGA, ICP-OES, calibration curve of copper, SEM and EDX mapping, Heterogenous nucleation of HKUST-1, BET linear plots and surface area analysis, and adsorption and desorption isotherms (PDF)

■ AUTHOR INFORMATION

Corresponding Author

*Email: ali.coskun@unifr.ch.

ORCID

Ali Coskun: 0000-0002-4760-1546

Notes

The authors declare no competing financial interest.

■ ACKNOWLEDGMENTS

We acknowledge support from the Swiss National Science Foundation for funding of this research (Grant 200021-175947).

■ REFERENCES

(1) Suh, M. P.; Park, H. J.; Prasad, T. K.; Lim, D. W. Hydrogen Storage in Metal-Organic Frameworks. *Chem. Rev.* **2012**, *112*, 782–835.

(2) Langmi, H. W.; Ren, J.; North, B.; Mathe, M.; Bessarabov, D. Hydrogen Storage in Metal-Organic Frameworks: AReview. *Electrochim. Acta* **2014**, *128*, 368–392.

(3) Ahmed, A.; Seth, S.; Purewal, J.; Wong-Foy, A. G.; Veenstra, M.; Matzger, A. J.; Siegel, D. J. Exceptional Hydrogen Storage Achieved by Screening Nearly Half a Million Metal-Organic Frameworks. *Nat. Commun.* **2019**, *10*, 1568.

(4) Ding, M.; Flaig, R. W.; Jiang, H.-L.; Yaghi, O. M. Carbon Capture and Conversion Using Metal–Organic Frameworks and MOF-based Materials. *Chem. Soc. Rev.* **2019**, *48*, 2783–2828.

(5) He, Y.; Zhou, W.; Qian, G.; Chen, B. Methane Storage in Metal–Organic Frameworks. *Chem. Soc. Rev.* **2014**, *43*, 5657–5678.

(6) Li, H.; Wang, K.; Sun, Y.; Lollar, C. T.; Li, J.; Zhou, H.-C. Recent Advances in Gas Storage and Separation Using Metal–Organic Frameworks. *Mater. Today* **2018**, *21*, 108–121.

(7) Li, J.-R.; Sculley, J.; Zhou, H.-C. Metal–Organic Frameworks for Separations. *Chem. Rev.* **2012**, *112*, 869–932.

(8) Kalmutzki, M. J.; Diercks, C. S.; Yaghi, O. M. Metal–Organic Frameworks for Water Harvesting From Air. *Adv. Mater.* **2018**, *30*, 1704304.

(9) Drout, R. J.; Robison, L.; Farha, O. K. Catalytic Applications of Enzymes Encapsulated in Metal–Organic Frameworks. *Coord. Chem. Rev.* **2019**, *381*, 151–160.

(10) Zhu, L.; Liu, X.-Q.; Jiang, H.-L.; Sun, L.-B. Metal–Organic Frameworks for Heterogeneous Basic Catalysis. *Chem. Rev.* **2017**, *117*, 8129–8176.

(11) Yang, Q.; Xu, Q.; Jiang, H.-L. Metal–Organic Frameworks Meet Metal Nanoparticles: Synergistic Effect for Enhanced Catalysis. *Chem. Soc. Rev.* **2017**, *46*, 4774–4808.

(12) Simmons, J. M.; Yildirim, T.; Hamaed, A.; Antonelli, D. M.; Webb, M. I.; Walsby, C. J. Direct Observation of Activated Hydrogen Binding to a Supported Organometallic Compound at Room Temperature. *Chem. - Eur. J.* **2012**, *18*, 4170–4173.

(13) Dinca, M.; Dailly, A.; Liu, Y.; Brown, C. M.; Neumann, D. A.; Long, J. R. Hydrogen Storage in a Microporous Metal-Organic Framework With Exposed Mn^{2+} Coordination Sites. *J. Am. Chem. Soc.* **2006**, *128*, 16876–16883.

(14) Chui, S. S.; Lo, S. M.; Charmant, J. P.; Orpen, A. G.; Williams, I. D. A Chemically Functionalizable Nanoporous Material. *Science* **1999**, *283*, 1148–1150.

(15) Lee, Y. G.; Moon, H. R.; Cheon, Y. E.; Suh, M. P. A Comparison of the H_2Sorption Capacities of Isostructural Metal–Organic Frameworks With and Without Accessible Metal Sites: $[\{Zn_2(abtc)(dmf)_2\}_3]$ and $[\{Cu_2(abtc)(dmf)_2\}_3]$ versus $[\{Cu_2(abtc)\}_3]$. *Angew. Chem., Int. Ed.* **2008**, *47*, 7741–7745.

(16) Moellmer, J.; Moeller, A.; Dreisbach, F.; Glaeser, R.; Staudt, R. High Pressure Adsorption of Hydrogen, Nitrogen, Carbon Dioxide and Methane on the Metal–Organic Framework HKUST-1. *Microporous Mesoporous Mater.* **2011**, *138*, 140–148.

(17) Kim, D.; Song, K. S.; Buyukcakir, O.; Yildirim, T.; Coskun, A. Bimetallic Metal Organic Frameworks With Precisely Positioned Metal Centers for Efficient H_2Storage. *Chem. Commun.* **2018**, *54*, 12218−12221.
(18) Parlett, C. M.; Wilson, K.; Lee, A. F. Hierarchical Porous Materials: Catalytic Applications. *Chem. Soc. Rev.* **2013**, *42*, 3876−3893.
(19) Furukawa, S.; Reboul, J.; Diring, S.; Sumida, K.; Kitagawa, S. Structuring of Metal−Organic Frameworks at the Mesoscopic/Macroscopic scale. *Chem. Soc. Rev.* **2014**, *43*, 5700−5734.
(20) Liu, D.; Zou, D.; Zhu, H.; Zhang, J. Mesoporous Metal−Organic Frameworks: Synthetic Strategies and Emerging Applications. *Small* **2018**, *14*, 1801454.
(21) Luo, Y.; Ahmad, M.; Schug, A.; Tsotsalas, M. Rising Up: Hierarchical Metal−Organic Frameworks in Experiments and Simulations. *Adv. Mater.* **2019**, *31*, 1901744.
(22) Yuan, S.; Zou, L.; Qin, J.-S.; Li, J.; Huang, L.; Feng, L.; Wang, X.; Bosch, M.; Alsalme, A.; Cagin, T.; Zhou, H.-C. Construction of Hierarchically Porous Metal−Organic Frameworks Through Linker Labilization. *Nat. Commun.* **2017**, *8*, 15356.
(23) Yang, J.; Zhang, Y.-B.; Liu, Q.; Trickett, C. A.; Gutiérrez-Puebla, E.; Monge, M. A.; Cong, H.; Aldossary, A.; Deng, H.; Yaghi, O. M. Principles of Designing Extra-Large Pore Openings and Cages in Zeolitic Imidazolate Frameworks. *J. Am. Chem. Soc.* **2017**, *139*, 6448−6455.
(24) Fang, Z.; Dürholt, J. P.; Kauer, M.; Zhang, W.; Lochenie, C.; Jee, B.; Albada, B.; Metzler-Nolte, N.; Pöppl, A.; Weber, B.; et al. Structural Complexity in Metal−Organic Frameworks: Simultaneous Modification of Open Metal Sites and Hierarchical Porosity by Systematic Doping With Defective Linkers. *J. Am. Chem. Soc.* **2014**, *136*, 9627−9636.
(25) Koo, J.; Hwang, I.-C.; Yu, X.; Saha, S.; Kim, Y.; Kim, K. Hollowing Out MOFs: Hierarchical Micro-and Mesoporous MOFs with Tailorable Porosity *via* Selective Acid Etching. *Chem. Sci.* **2017**, *8*, 6799−6803.
(26) Shen, K.; Zhang, L.; Chen, X.; Liu, L.; Zhang, D.; Han, Y.; Chen, J.; Long, J.; Luque, R.; Li, Y.; Chen, B. Ordered Macro-Microporous Metal-Organic Framework Single Crystals. *Science* **2018**, *359*, 206−210.
(27) Qiu, L. G.; Xu, T.; Li, Z. Q.; Wang, W.; Wu, Y.; Jiang, X.; Tian, X. Y.; Zhang, L. D. Hierarchically Micro-and Mesoporous Metal−Organic Frameworks With Tunable Porosity. *Angew. Chem., Int. Ed.* **2008**, *47*, 9487−9491.
(28) Tan, Y. C.; Zeng, H. C. Defect Creation in HKUST-1 via Molecular Imprinting: Attaining Anionic Framework Property and Mesoporosity for Cation Exchange Applications. *Adv. Funct. Mater.* **2017**, *27*, 1703765.
(29) Duan, C.; Zhang, H.; Yang, M.; Li, F.; Yu, Y.; Xiao, J.; Xi, H. Templated Fabrication of Hierarchically Porous Metal−Organic Frameworks and Simulation of Crystal Growth. *Nanoscale Adv.* **2019**, *1*, 1062−1069.
(30) Petit, C.; Burress, J.; Bandosz, T. J. The Synthesis and Characterization of Copper-based Metal−Organic Framework/Graphite Oxide Composites. *Carbon* **2011**, *49*, 563−572.
(31) Wang, Q.; Yang, Y.; Gao, F.; Ni, J.; Zhang, Y.; Lin, Z. Graphene Oxide Directed One-step Synthesis of Flowerlike Graphene@HKUST-1 for Enzyme-free Detection of Hydrogen Peroxide in Biological Samples. *ACS Appl. Mater. Interfaces* **2016**, *8*, 32477−32487.
(32) Petit, C.; Bandosz, T. J. MOF-Graphite Oxide Composites: Combining the Uniqueness of Graphene Layers and Metal-Organic Frameworks. *Adv. Mater.* **2009**, *21*, 4753−4757.
(33) Muschi, M.; Serre, C. Progress and Challenges of Graphene Oxide/Metal-Organic Composites. *Coord. Chem. Rev.* **2019**, *387*, 262−272.
(34) Li, Y.; Miao, J.; Sun, X.; Xiao, J.; Li, Y.; Wang, H.; Xia, Q.; Li, Z. Mechanochemical Synthesis of Cu-BTC@GO With Enhanced Water Stability and Toluene Adsorption Capacity. *Chem. Eng. J.* **2016**, *298*, 191−197.
(35) Kumar, R.; Raut, D.; Ramamurty, U.; Rao, C. N. R. Remarkable Improvement in the Mechanical Properties and CO_2 Uptake of MOFs Brought About by Covalent Linking to Graphene. *Angew. Chem., Int. Ed.* **2016**, *55*, 7857−7861.
(36) Kim, D.; Kim, D. W.; Hong, W. G.; Coskun, A. Graphene/ZIF-8 Composites With Tunable Hierarchical Porosity and Electrical Conductivity. *J. Mater. Chem. A* **2016**, *4*, 7710−7717.
(37) Jahan, M.; Bao, Q. L.; Yang, J. X.; Loh, K. P. Structure-Directing Role of Graphene in the Synthesis of Metal-Organic Framework Nanowire. *J. Am. Chem. Soc.* **2010**, *132*, 14487−14495.
(38) Cortés-Súarez, J.; Celis-Arias, V.; Beltrán, H. I.; Tejeda-Cruz, A.; Ibarra, I. A.; Romero-Ibarra, J. E.; Sánchez-González, E.; Loera-Serna, S. Synthesis and Characterization of an SWCNT@HKUST-1 Composite: Enhancing the CO_2 Adsorption Properties of HKUST-1. *ACS Omega* **2019**, *4*, 5275−5282.
(39) Qiu, X.; Wang, X.; Li, Y. Controlled Growth of Dense and Ordered Metal-Organic Framework Nanoparticles on Graphene Oxide. *Chem. Commun.* **2015**, *51*, 3874−3877.
(40) Van Vleet, M. J.; Weng, T.; Li, X.; Schmidt, J. In Situ, Time-Resolved, and Mechanistic Studies of Metal−Organic Framework Nucleation and Growth. *Chem. Rev.* **2018**, *118*, 3681−3721.
(41) Bagri, A.; Mattevi, C.; Acik, M.; Chabal, Y. J.; Chhowalla, M.; Shenoy, V. B. Structural Evolution During The Reduction of Chemically Derived Graphene Oxide. *Nat. Chem.* **2010**, *2*, 581−587.
(42) Gadipelli, S.; Lu, Y.; Skipper, N. T.; Yildirim, T.; Guo, Z. X. Design of Hyperporous Graphene Networks and Their Application in Solid-Amine Based Carbon Capture Systems. *J. Mater. Chem. A* **2017**, *5*, 17833−17840.
(43) Krawiec, P.; Kramer, M.; Sabo, M.; Kunschke, R.; Fröde, H.; Kaskel, S. Improved Hydrogen Storage in the Metal-Organic Framework $Cu_3(BTC)_2$. *Adv. Eng. Mater.* **2006**, *8*, 293−296.
(44) Panella, B.; Hirscher, M.; Pütter, H.; Müller, U. Hydrogen Adsorption in Metal−Organic Frameworks: Cu-MOFs and Zn-MOFs Compared. *Adv. Funct. Mater.* **2006**, *16*, 520−524.
(45) Hummers Jr, W. S.; Offeman, R. E. Preparation of Graphitic Oxide. *J. Am. Chem. Soc.* **1958**, *80*, 1339−1339.